Effect of Chloride on the Pitting Corrosion of Carbon Steel in Alkaline Solutions

Journal of The Electrochemical Society, 2022 **169** 031501
1945-7111/2022/169(3)/031501/7/$40.00 © 2022 The Electrochemical Society ("ECS"). Published on behalf of ECS by IOP Publishing Limited

Effect of Chloride on the Pitting Corrosion of Carbon Steel in Alkaline Solutions

Jie Qiu,[1,2,z] Yakun Zhu,[1] Yi Xu,[1] Yanhui Li,[3] Feixiong Mao,[4] Angjian Wu,[1] and Digby D Macdonald[1,*,z]

[1]*Departments of Nuclear Engineering, University of California at Berkeley, Berkeley, California 94720, United States of America*
[2] *School of Nuclear Science and Technology, Xi'an Jiaotong University, Xi'an 710049, People's Republic of China*
[3]*Key Laboratory of Thermo-Fluid Science and Engineering of MOE, School of Energy and Power Engineering, Xi'an Jiaotong University, Xi'an 710049, People's Republic of China*
[4]*Ningbo Key Laboratory of Marine Protection Materials, Ningbo Institute of Materials Technology and Engineering, Chinese Academy of Sciences, Ningbo 315201, People's Republic of China*

The effect of chloride concentration on the passivity breakdown of carbon steel in deaerated pH = 13.5 alkaline solution was investigated. The results show that chloride plays an important role for the pitting corrosion of carbon steel. When NaCl ⩽ 1 M, the carbon steel is passive but for 1 M< NaCl < 2 M, the carbon steel transfers from passive to passivity breakdown. When NaCl ⩾ 2 M, passive film breakdown occurs and the passivity breakdown potential (E_b) of carbon steel is linearly-dependent on the logarithm of the chloride activity in the alkaline solution. As predicted by the PDM, the near-normal distribution of E_b is well indicated by the near straight line in the cumulative distribution probability. The analysis in this study gives us a method to calculate the E_b of carbon steel in alkaline solution and its distribution for any given chloride concentration.
 [DOI: 10.1149/1945-7111/ac580c]

Manuscript submitted November 21, 2021; revised manuscript received January 10, 2022. Published March 4, 2022.

Carbon steel is chosen as a candidate overpack material for the supercontainer for the disposal of high-level nuclear waste (HLNW).[1–3] In the supercontainer, the carbon steel overpack contains the HLNW and is located concentrically in an outer stainless-steel envelope that isolates the overpack from direct contacts with the environment. The annulus between the overpack and the outer steel envelop is filled with a concrete material, which is similar to the Portland Type I cement concrete.[3] The outside of the carbon steel overpack is therefore in contact with concrete pore water, which is a high pH of 13.5 alkaline solution that is simulated by saturated $Ca(OH)_2$ containing sufficient NaOH to adjust the pH to 3.5 at 25 °C.[4] The details of the geometry and dimensions of the HLNW supercontainer can be seen from Ref. 5. It is well known that carbon steel can spontaneous form an ultra-thin passive film on its surface that acts as a barrier protect metal from corrosion when in contact with high pH concrete buffer solution.[6,7] However, chloride, a common, deleterious contaminant in the concrete, is capable of inducing passive breakdown and leading to the active corrosion of carbon steel.[8–11] Pitting corrosion is a main potential threat to the integrity of the carbon steel overpack when it contains the HLNW over the extended storage time (e.g. >100,000 years).

Over the past few decades, the effect of chloride on the corrosion behavior of carbon steel in concrete or in simulated concrete pore solution (SCPS) has been extensively studied.[9–19] However, most of this research concerns the corrosion of carbon steel rebar in concrete, in which the concrete solution is open to the air and contains a high oxygen content.[17–19] Unlike the carbon steel rebar case, the carbon steel overpack will be contained in a steel envelop in the HLNW supercontainer. The oxygen gas trapped inside the concrete material between the overpack and the outer steel envelop will be gradually consumed by the oxidation of materials (e.g. corrosion of the steel) and microbial activity and finally forms an anoxic environment. At the same time, the decreasing oxygen partial pressure inside the annulus will decrease the corrosion potential of carbons steel and render hydrogen evolution by the reduction of water viable when the potential is sufficient negative.[20] It is known that the gas tightness of the steel envelope is sufficiently good, H_2 cannot escape, and air cannot enter, the annulus between the carbon steel overpack and steel envelope will become an anoxic and be pressurized with H_2.[2]

It is known that the oxygen concentration in the solution influences the formation of the passive film and affects the corrosion potential of carbon steel in alkaline solution.[16] For example, Alhozaimy et al.[21] found that the dissolved oxygen concentration is crucial for the proper formation of the passive layer of steel in concrete solutions, and the corrosion rate of rebar in adequately oxygenated solution is lower than that in lower oxygen concentration solution. Doi et al.[22] reveal that the charge transfer resistance of the carbon steel under excessively high oxygen concentration is higher in comparison to that at lower oxygen pressure, because of the formation of a protective passive film under the excessive supply of oxygen. Actually, the corrosion of carbon steel in alkaline solution includes the anodic dissolution of iron and the cathodic reduction of oxygen or water. Depending on the oxygen concentration, the cathodic reaction plays an important role in the corrosion of carbon steel in concrete. To our knowledge, there are only limited research that focused on the corrosion of carbon steel under anoxic conditions, which is relevant to the disposal of HLNW. Thus, systematic and in-depth study the effect of chloride on the corrosion of carbon steel in alkaline solution under anoxic condition is crucial to ensure the safe application of carbon steel for the disposal of HLNW.

In this study, we report the potentiodynamic polarization study of carbon steel in alkaline solution as a function of chloride concentration. The passivity breakdown potential of the passive film was measured as a function of chloride concentration over a wide range of concentration. The effect of chloride on the pitting corrosion of carbon steel in alkaline solution was analyzed in terms of the Point Defect Model (PDM). Besides being significant for the disposal of HLNW, this work is also helpful for predicting the corrosion of rebar in reinforced concrete structures.

Experimental

A traditional three electrode cell was used for the electrochemical experiments in this work. The working electrode (WE) was P355 QL2 carbon steel, that was provided by ONDARF/NIRAS of Belgium. A saturated calomel electrode (SCE) and a nickel gauze were chosen as the reference electrode (RE) and counter electrode (CE), respectively. The carbon steel samples are small cylinders with diameters of 5 mm and lengths of 10 mm. Table I shows the chemical composition of the P355 QL2 carbon steel. For the WE, the samples were mounted in epoxy resin and with an area of 0.196 cm^2 exposed to the solution. Prior to the electrochemical

*Electrochemical Society Fellow.
[z]E-mail: qiujie@berkeley.edu; macdonald@berkeley.edu

Table I. Chemical composition of the P355 QL2 carbon steel used in this study (wt.%).

C	Mn	P	Si	Cu	Ni	Cr	Mo	Al	Nb	Fe
0.15	0.98	0.005	0.324	0.043	0.05	0.082	0.009	0.034	0.006	Bal.

experiments, the sample was ground with SiC abrasive papers down to 2500 grit, then was rinsed with ethanol and deionized water.

The experimental solutions were saturated $Ca(OH)_2$ + 0.43 M NaOH containing different sodium chloride concentrations of 0 M, 0.1 M, 0.5 M, 1 M, 1.5 M, 2 M, 3.5 M and 5.4 M (saturated), in which the pH were calculated using OLI System's software to be 13.5 at 25 °C. Prior to the experiments, all the solutions were purged with ultrahigh purity N_2 + 4% H_2 (UHP 99.999%) for 5 h at a high flow rate to expel oxygen. After this, we dipped the WE into the solution and purged another 20 min to expel extra oxygen before starting experiment. The deaeration was continued during the electrochemical measurements by slowly flowing gas at 15 ml min^{-1}. The hydrogen was added to simulate the condition of the concrete between carbon steel overpack and steel envelope of the supercontainer and keep a well-defined equilibrium potential for the hydrogen electrode reaction. The temperature of the solution was controlled at 25 °C using a water bath.

All the electrochemical measurements were measured using a Gamry Interface 1000 potentiostat. After putting the specimen in the electrolyte, the samples were cathodically polarized at −1.2 V_{SCE} for 5 min to remove the air-formed oxide film. Then the samples were exposed in the solutions for 1 h to establish a stable open circuit potential (OCP) prior to potentiodynamic polarization. The potentiodynamic polarization was measured from −1.2 V_{SCE} to 0.7 V_{SCE} at a sweep rate of 0.1667 mV s^{-1} to determine the passivity breakdown potential (E_b) of the carbon steel in the simulated CPS. The potentiodynamic polarization were repeated 15 times for each solution to obtain the statistical distribution of E_b. Electrochemical impedance spectroscopy (EIS) was measured at the OCP over a frequency range from 100 kHz to 10 mHz. The amplitude of the perturbation voltage was 10 mV.

Results

The potentiodynamic polarization curves of carbon steel in deaerated alkaline solution at 25 °C as a function of chloride concentration are shown in Fig. 1. From the cyclic potentiodynamic polarization plots, the zero current potential of carbon steel is around −1.0 V_{SCE} in the solution deaerated with N_2 + 4% H_2. When the chloride concentration is lower or equal than 1 M, a wide passive region (from −1.0 V_{SCE} to 0.5 V_{SCE}) is observed in the polarization curves, and no passivity breakdown occurs for carbon steel with NaCl $\leqslant$ 1 M, as evidenced by the lack of positive hysteresis on the reverse sweep. Note that the sharp increase in the current density at 0.5 V_{SCE} is induced by oxygen evolution reaction (OER).[23] When the chloride concentration is higher than 2 M, the passive film breakdown occurs as is evidenced by the positive hysteresis on the reverse sweep, and the passivity breakdown potential decreases with increasing chloride concentration. Moreover, metastable pitting as indicated by the short period current spikes in the passive region appeared for carbon steel in alkaline solution with NaCl $\geqslant$ 2 M, which is due to breakdown of passive film followed immediately by repassivation.

To further explore the processes that occur between 1 M to 2 M, we measured the polarization curves of carbon steel in the alkaline solution with 1.5 M NaCl. The results show that the polarization behavior of carbon steel in this case is somewhat inconsistent, because sometimes the passive film breaks and sometimes it does not. Figure 2 shows two typical polarization plots under nominally identical conditions, it is seen from the black line that the carbon steel remains passive until oxygen evolution occurs. Contrariwise, from the red line in Fig. 2, we can see that passivity breakdown

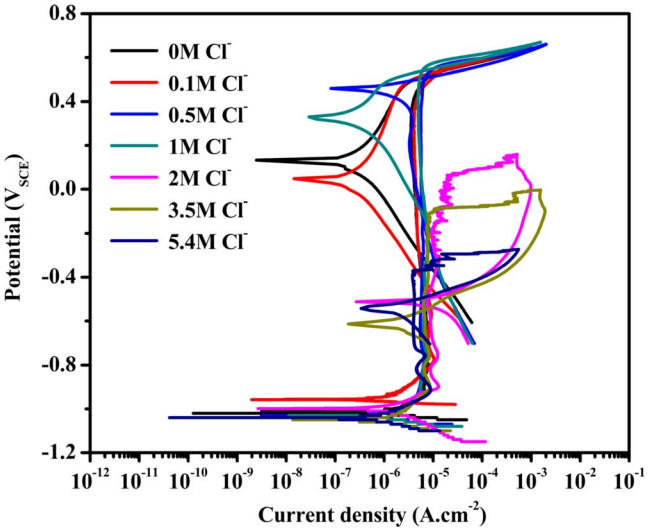

Figure 1. Potentiodynamic polarization curves of carbon steel in the deaerated alkaline solution (pH = 13.5, at 25 °C) with different chloride content (scan rate of 0.1667 mV s^{-1}).

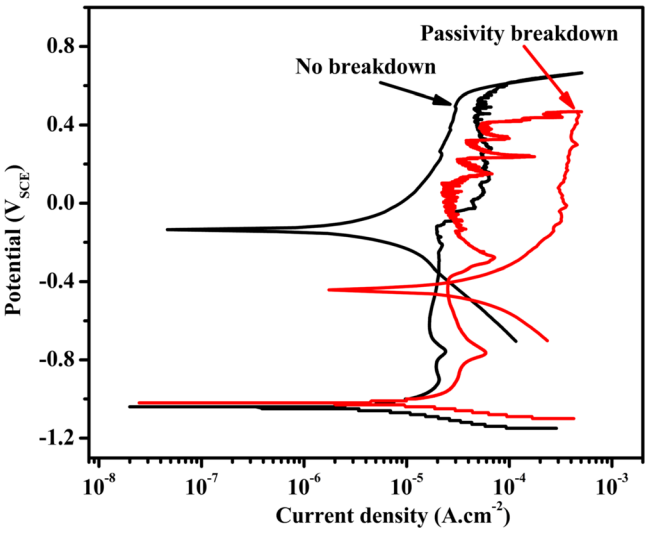

Figure 2. Potentiodynamic polarization curves of carbon steel in the deaerated alkaline solution (pH = 13.5, at 25 °C) with 1.5 M NaCl (scan rate of 0.1667 mV s^{-1}).

occurs, resulting in positive hysteresis on the reverse potential sweep, giving rise to stable pitting with an E_b of around 0.4 V_{SCE}. Metastable pitting events, which appear as short period current changes, are observed in both polarization plots when the potential is higher than −0.2 V_{SCE}. Based on the results, it is apparent that a chloride concentration between 1 M to 2 M is a transition zone, where the carbon steel transfers from the passive state to pitting corrosion in the pH = 13.5 alkaline solution at 25 °C.

Passivity breakdown was observed when the chloride concentration in the solution is higher than 2 M. To investigate the effect of chloride on E_b and also to obtain the statistical distributions of E_b, a set of 15 replicate polarization experiments were performed in the

alkaline solution with different chloride concentration, and the results are presented in Fig. 3. It can be seen that, in all cases, the positive hysteresis in the cycle polarization plots clearly indicates stable pitting corrosion. The E_b decreases with increasing chloride concentration in the solution.

According to the above polarization results, the mean values of the passivity breakdown potentials of carbon steel in pH = 13.5 alkaline solution at 25 °C as a function of chloride concentrations is shown in Fig. 4. It can be seen that the curve can be divided into three sections, and the transition from passivity to pitting corrosion displays a "Z-shaped" curve. When NaCl $\leqslant$ 1 M, the carbon steel is passive in the alkaline solution and no passivity breakdown occurs. The "breakdown" potential shown in this case is not due to the breakdown of the passive film but is the potential corresponding to the onset of the oxygen evolution reaction (OER). When 1 M < NaCl < 2 M, the carbon steel transfers from passivity-to-passivity breakdown but whether passivity breakdown occurs is a matter of statistics, as discussed below. The passivity behavior is influenced by time, temperature, surface conditions, oxygen concentration and so on. When NaCl $\geqslant$ 2 M, the passive film breakdown occurs unequivocally and the E_b decrease with increasing chloride concentration. These results indicate that chloride plays an important role for the pitting corrosion of carbon steel in concrete solutions.

In order to further confirm the effect of chloride on the corrosion behavior of carbon steel, the EIS of carbon steel in the deaerated alkaline solutions were measured at OCP and the results are shown in Fig. 5. Within experimental uncertainty, it is seen that the impedance modulus of carbon steel decreases with increasing the chloride concentration of the solution (Fig. 5a). As shown in Fig. 5b, the Nyquist plots are composed of a line that is induced by diffusion process and a semicircle. Within experimental uncertainty, we can find the radius of the semi-circle, corresponds to the resistance of the passive film, decreases with increasing the concentration of the chloride in the solution. These trends indicate that chloride generates a negative effect on the corrosion resistance of the passive film on carbon steel, which is consistent with the above potentiodynamic polarization results.

Discussion

It is well known that carbon steel spontaneously forms a protective passive film when it is exposed to high pH solution.[24,25] The passive film of carbon steel generally comprises a highly point defective inner barrier layer and a porous precipitated outer layer. Chloride has a remarkable ability to cause pitting corrosion of carbon steel because of a judicious combination of a relatively low dehydration energy, little need to expand a surface oxygen vacancy to accommodate Cl^-, and a favorable insertion energy of the anion into the vacancy.[12,26] The PDM, developed by Macdonald et al.,[27] has been successfully used to describe passivity and passivity breakdown, and will be used to analyze the effect of chloride on pitting corrosion of carbon steel here. In the PDM, seven reactions account for the generation and annihilation of point defects and are

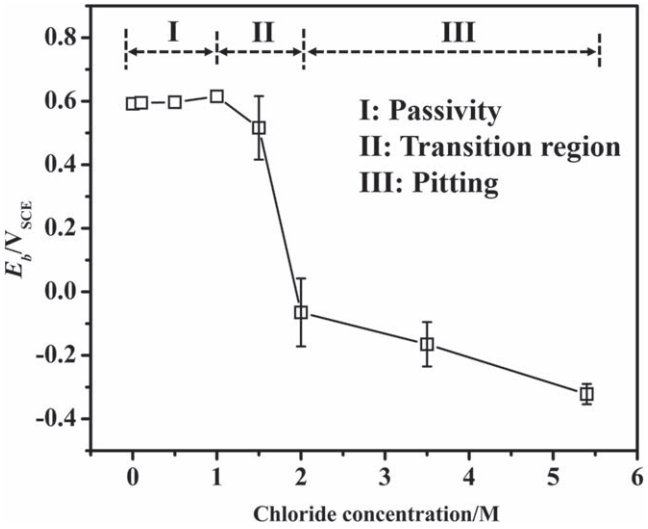

Figure 4. Mean values of the passivity breakdown potentials (E_b) of carbon steel in pH = 13.5 alkaline solution at 25 °C as a function of chloride concentrations.

responsible for passive and passivity breakdown of passive film. Figure 6 shows schematically the process leading to the breakdown of passive films on carbon steel in concrete pore solution in terms of PDM. According to the PDM, of the seven reactions in the PDM, only Reactions 1 and 4 are related with the breakdown of barrier layer of the passive film. To simplify the following discussion, we present only Reactions 1 and 4 of PDM in Fig. 6. Full details of the PDM are given in Ref. 28.

Noting that the oxygen vacancy ($V_O^{\cdot\cdot}$) has a formal positive charge +2, the anion Cl^- is readily absorbed into an oxygen vacancy at the barrier layer/solution (bl/s) interface through the following reaction:[10]

$$V_O^{\cdot\cdot} + Cl^- \rightarrow Cl_O^{\cdot} \quad [1]$$

When the oxygen vacancy absorbs Cl^-, the cation vacancy at the bl/s interface increases by the following autocatalytic Schottky pair reaction:

$$\text{Null} \leftrightarrow V_M^{\chi'} + \frac{\chi}{2} V_O^{\cdot\cdot} \quad [2]$$

or by a chloride-mediated cation extraction reaction to produce a $V_M^{\chi'} V_O^{\cdot\cdot}$ pair and regenerate Cl^-.[29]

$$M_M Cl_O^{\cdot} + nH_2O \rightarrow V_M^{\chi'} V_O^{\cdot\cdot} + M_s^{\chi+}.nH_2O + Cl^- \quad [3]$$

The movement of a cation from the layer beneath the surface regenerates the oxygen vacancy from the $V_M^{\chi'} V_O^{\cdot\cdot}$ pair, where $V_M^{\chi'}$ and

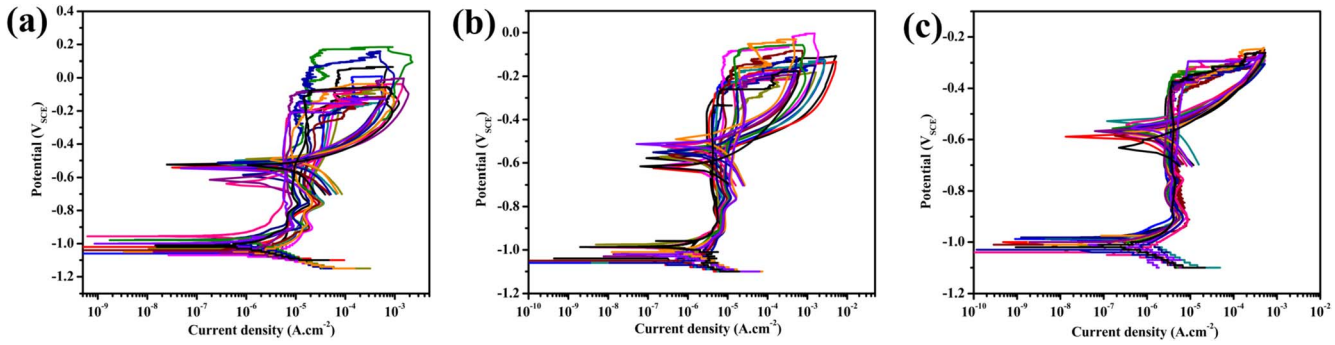

Figure 3. Potentiodynamic polarization curves of carbon steel in the deaerated alkaline solution (pH = 13.5, at 25 °C) with (a) 2 M NaCl, (b) 3.5 M NaCl and (c) 5.4 M NaCl.

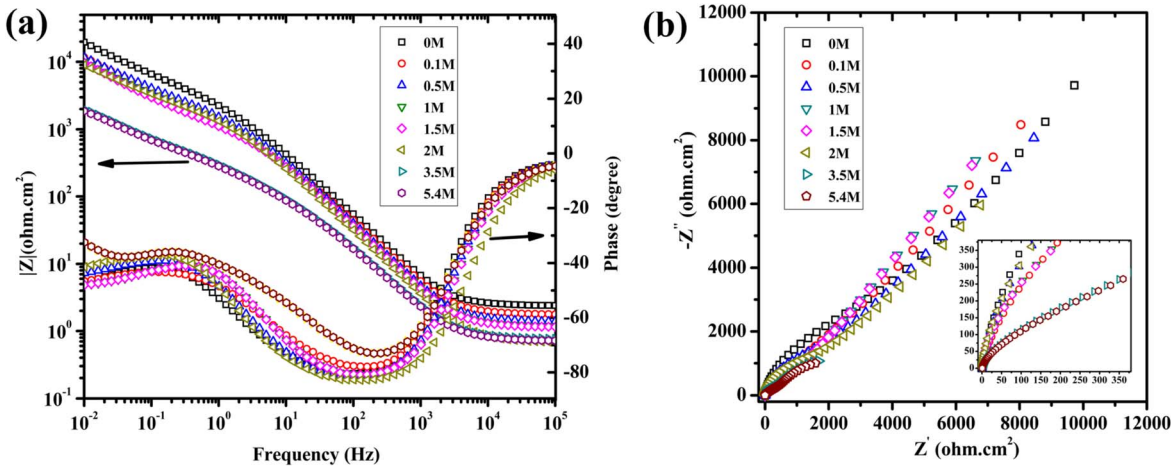

Figure 5. EIS plots of carbon steel in the deaerated alkaline solution (pH = 13.5, at 25 °C) with different chloride concentrations (a) Nyquist and (b) Bode plots.

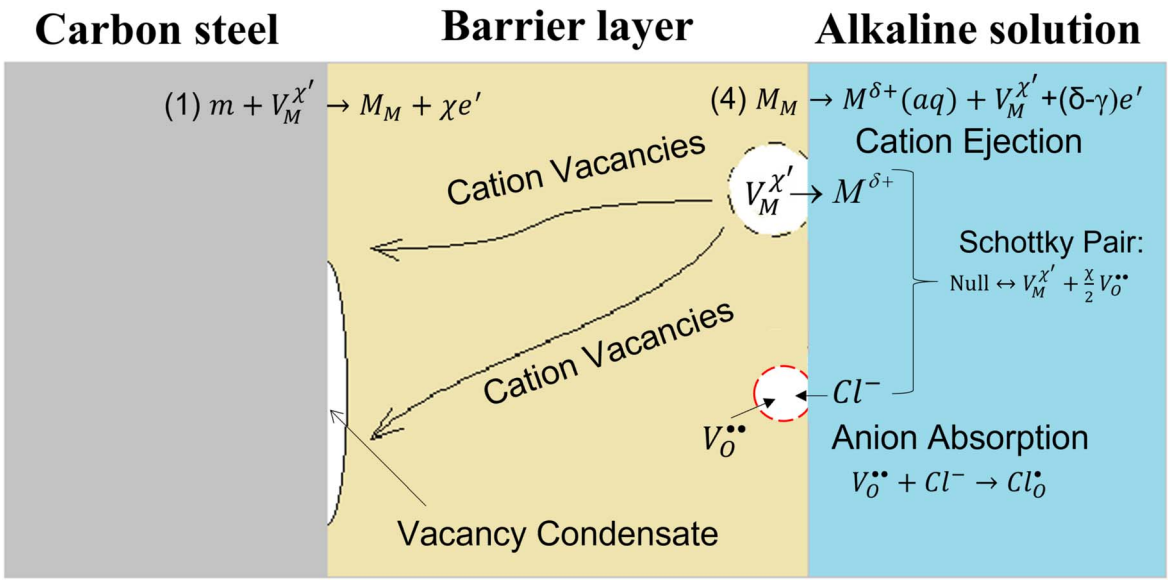

Figure 6. The processes leading to the breakdown of passive films on carbon steel in alkaline solution.

M_M are the cation vacancy and metal cation in the surface of the barrier layer, respectively. Thus, the generation of cation vacancies at the bl/s interface is autocatalytic in both Cl^- and $V_O^{\bullet\bullet}$. This accounts for the fact that chloride is never consumed when initiating passivity breakdown and why the absorption of chloride occurs at the periphery of the vacancy condensate (see below) and why the absorbed Cl^- redistributes to the edge of the condensate as the condensate grows in size. This is because cation vacancy condensation occurs at the periphery of the blister and it is at this location that the above reactions occur at the bl/s interface. The increase in the cation vacancy concentration enhances the flux of vacancies migrating from the bl/s interface to the metal/barrier layer (m/bl) interface. Under the non-breakdown situation (i.e. NaCl $\leqslant 1\,M$ in this study), the cation vacancies are promptly annihilated at the m/bl interface through injection of cation atoms from the carbon steel matrix by the following reaction (i.e. Reaction 1 in Fig. 6):

$$m + V_M^{\chi'} \rightarrow M_M + \chi \text{ the non-breakdown} \qquad [4]$$

where m is metal atom (i.e. Fe in this study), $V_M^{\chi'}$ and M_M are the cation vacancy and metal cation in the barrier layer, respectively. As the pH of the solution is basically unchanged (OH^- is constant), more oxygen vacancies absorb Cl^- with increasing the chloride concentration, and therefore more cation vacancies will be formed and migrates to the m/bl interface. If the flux of cation vacancies to the m/bl interface is sufficiently high, and the cation vacancies cannot be promptly annihilated by Reaction 4. Consequently, the extra cation vacancies condense at the m/bl interface to form a blister that results in the separation of barrier layer from the metal matrix, as shown in Fig. 6. As time goes on, the blister continue grows by the condensation of cation vacancies at the periphery, as noted above. However, the passive film stops growing due to the separation of barrier layer from carbon steel matrix, but the passive film continues to dissolve and gets thinner. Eventually, the passive film ruptures due to the growth stresses, reducing a passivity breakdown. It should be noted here that both mechanisms for cation vacancy generation at the bl/s interface outlined above (the Schottky pair reaction and the chloride (anion)-mediated cation extraction reaction) lead to the same relationships between the breakdown voltage and induction time and the various independent variables (Cl^-, pH, potential, etc.), but of course the two models contain different parameters. Although the Schottky pair model for cation vacancy generation was first proposed in 1981,[30] we consider the chloride (anion)-mediated cation extraction mechanism to be the more physically realistic. However, for historical reasons, we will present the original treatment here.

According to PDM, the relationship between critical breakdown potential and chloride concentration could be expressed as follows:[27]

$$E_b = \frac{4.606RT}{\chi\alpha F}\log\left(\frac{\lambda}{\bar{D}}\right) - \frac{2.303RT}{\alpha F}\log\left(a_{X^-}\right) \quad [5]$$

where

$$\lambda = \frac{RTJ_m\Omega}{\chi F\varepsilon N_A}\exp\left[\frac{\Delta G_S^0 + \left(\frac{\chi}{2}\right)\Delta G_A^0 - \left(\frac{\chi}{2}\right)\beta FpH - \left(\frac{\chi}{2}\right)F\phi_{\frac{f}{s}}^0}{RT}\right] \quad [6]$$

and F is Faraday's constant, R is the gas constant, T is the temperature in Kelvin, α is the polarizability constant that correlates the potential drop across the bl/s interface with the applied voltage, J_m is the rate of annihilation of cation vacancies at the m/bl interface, χ is the stoichiometry of the oxide film (charge number on the cation), Ω is the mole volume of the oxide per cation ($MO_{\chi/2}$), D is the diffusivity of the cation vacancy in the barrier layer, ε is the electric field strength, $\phi_{f/s}^0$ is the potential drop across the bl/s interface at $E = 0$ and pH = 0, N_A is the Avogadro's number, ΔG_S^0 is the change in standard Gibbs energy for the generation of cation vacancy/oxygen vacancy pairs, ΔG_A^0 is the corresponding term for absorption of a Cl^- into an oxygen vacancy in the surface of the passive film, and a_{X^-} is the activity of chloride. According to the potentiodynamic polarization results in Fig. 3, the average E_b of carbon steel in the pH = 13.5 alkaline solution contains 2 M, 3.5 M and 5.4 M NaCl are -0.082 ± 0.107 V_{SCE}, -0.165 ± 0.071 V_{SCE} and -0.302 ± 0.032 V_{SCE}, respectively. Figure 7 shows the relationship between E_b of carbon steel and logarithm of the chloride activity of the solution. As expected, the linear dependence of E_b on $\log(a_{X^-})$ is observed. By fitting using Eq. 5, the E_b as a function of $\log(a_{X^-})$ can be described as:

$$E_b = 0.065 - 0.457\log\left(a_{X^-}\right) \quad [7]$$

By comparing Eqs. 7 and 5, we obtain that $\alpha = 0.13$, which agrees well with the value from the literature ($\alpha = 0.16$).[9,31]

It is known that the breakdown potential of alloy follows a near normal distribution, as has been observed experimentally, due to the exist of many active cites in the barrier layer.[32] These sites correspond to local regions of high structural disorder, such as at the boundaries between inclusions (e.g., MnS) and precipitates (e.g. $Cr_{23}C_6$) that project through the barrier layer, within which the cation vacancy diffusivity is significantly higher than in the surrounding barrier layer. Assuming a random distribution of the potential breakdown sites with respect to the cation vacancy diffusivity (D), the population of breakdown sites can be expressed as the normal distribution function:[33]

$$\frac{dN}{dD} = \frac{1}{\sqrt{2\pi}\sigma_D}\exp\left(\frac{-(D-\bar{D})^2}{2\sigma_D}\right) \quad [8]$$

where $\bar{D}$ is the mean value of diffusivity of the cation vacancy in the barrier layer, and σ_D is the standard deviation, which reflects the width of the normal distribution. The distribution of E_b is defined as:

$$\frac{dN}{dE_b} = \frac{dN}{dD}\Big/\frac{dE_b}{dD} \quad [9]$$

According to the PDM, by taking the derivative of Eq. 5 with respect to D, we can obtain:[33]

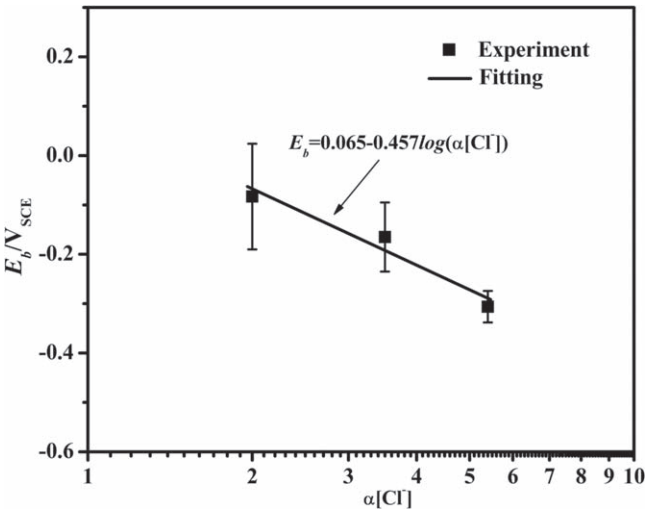

Figure 7. The dependence of the E_b of carbon steel in deaerated alkaline solution (pH = 13.5 at 25 °C) on chloride activity.

$$\frac{dE_b}{dD} = -\frac{D}{\gamma'} \quad [10]$$

Substitution of Eqs. 8 and 10 into Eq. 9 yields:

$$\frac{dN}{dE_b} = \frac{-b\gamma'}{\sqrt{2\pi}\sigma_D(a_X)^{\chi/2}}e^{-(e^{-\gamma' E_b}-e^{-\gamma'\bar{E}_b})^2 b^2/2\sigma_D(a_X)^{\chi}}e^{-\gamma' E_b} \quad [11]$$

where

$$\gamma' = \chi\alpha F/2RT \quad [12]$$

$$b = \bar{D}a_X^{\chi/2}e^{\gamma' E_b} \quad [13]$$

and $\bar{E}_b$ is the mean value of the E_b, which is expressed as:

$$\bar{E}_b = \frac{1}{\gamma'}\ln\left(\frac{ba_X^{\frac{\chi}{2}}}{\bar{D}}\right) \quad [14]$$

The cumulative distribution probability ($P(E_b)$) functions of the breakdown potential is defined as:

$$P(E_b) = 100 \times \int_{-\infty}^{E_b}\left(\frac{dN}{dE_b}\right)dE_b \Big/ \int_{-\infty}^{\infty}\left(\frac{dN}{dE_b}\right)dE_b \quad [15]$$

To investigate the distributions of E_b for carbon steel in alkaline solution, the cumulative distributions probability functions are shown in Fig. 8. Within the experimental uncertainty, the near-normal distribution of E_b is well indicated by the near straight line in the cumulative distribution probability function. In addition, E_b shifts to more negative potentials with increasing chloride concentration of the solution, in keeping with Eq. 13. To interpret the effect of chloride on the E_b, the E_b distribution data obtain in the solution with 2 M NaCl (black point in Fig. 8) was optimized using the Eq. 15, and the optimization line and parameters are shown in Fig. 8 and Table II, respectively. The parameters in Table II were then used to predict the cumulative distribution of E_b at 3.5 M NaCl and 5.4 M NaCl, and the calculated results are shown in Fig. 8 (solid line). The close agreement between the calculated results and the experimental data confirms of the validity of the PDM for describing the pitting corrosion of carbon steel in alkaline solution with aggressive chloride. The analysis in this study gives us a method to calculate

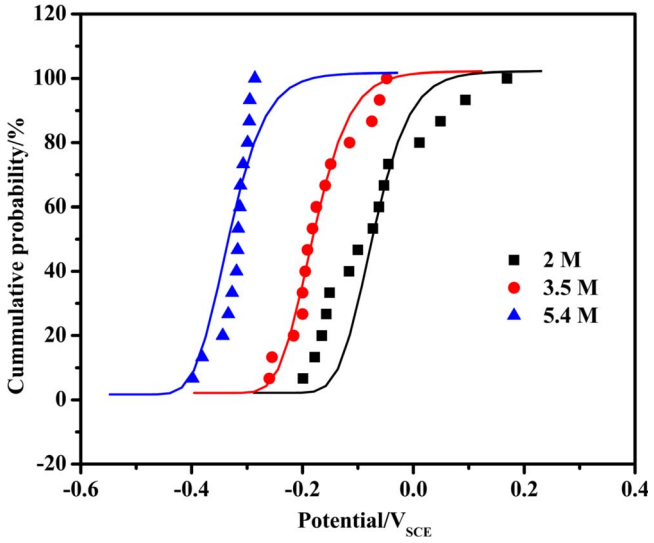

Figure 8. Calculated cumulative probability distributions of E_b for carbons steel in deaerated pH = 13.5 alkaline solution with different chloride content (compared with experimentally determined distributions). The solid lines are calculated results and the points are experimental data.

the E_b of carbon steel in simulated concrete pore solution for any given chloride concentration.

Returning now to Fig. 6, as the activity of chloride is reduced the measured breakdown potential increases sharply within the region II and the phenomenon at the interface that carries the current shifts from pitting to oxygen evolution. This shift is attributed to a lengthening of the induction time for pit nucleation. Thus, according to the PDM, the induction time for nucleation of a single pit as:[30]

$$t_{ind} = \xi'\left[\exp\left(\frac{\chi\alpha F\Delta V}{2RT}\right) - 1\right]^{-1} + \tau \qquad [16]$$

Where

$$\xi' = \xi/J^0 u^{-\chi/2}(a_{X^-})^{\chi/2}\exp\left(\frac{\alpha\chi FV_c}{2RT}\right) \qquad [17]$$

Note that V is the applied voltage, $\Delta V = V - V_c$, is the overpotential for pit nucleation, τ is the time from first vacancy condensation to rupture of the cap. The quantities J^0 and u are defined as:[12]

$$J^0 = \chi K D_{V_M^{\chi'}}(N_v/\Omega)^{(1+\chi/2)}\exp\left(-\Delta G_s^0/RT\right) \qquad [18]$$

and

$$u = \frac{N_v}{\Omega}\exp\left(\frac{\Delta G_A^0 - \beta FpH - F\phi_{f/s}^0}{RT}\right) \qquad [19]$$

As the overvoltage and or $a_X \to 0$, $t_{ind} \to \infty$ and because passivity breakdown was detected potentiodynamically, the shift in the breakdown potential reflects the fact that insufficient time is available for pits to nucleate so that the current becomes dominated by oxygen evolution. Accordingly, if a lower sweep rate were employed in measuring the breakdown potential, the PDM predicts that Region II, Fig. 6, will shift to lower [Cl$^-$]. At an infinitely low voltage sweep rate, the E_b vs Log([Cl$^-$]), Eq. 7, should extend into Region III to very low [Cl$^-$] provided that there are sufficient pits to carry the current.

Conclusions

In this study, the effect of chloride concentration on the passivity breakdown of carbon steel in deaerated pH = 13.5 alkaline solution was studied using potentiodynamic polarization. The main conclusions are as follows:

(1) Chloride plays an important role for the pitting corrosion of carbon steel in alkaline solutions and the effect of chloride on the pitting corrosion is divided into three sections. When NaCl $\leqslant$1 M, the carbon steel is passivated and no passivity breakdown occurs. When 1 M < NaCl < 2 M, the carbon steel transfers from passivity-to-passivity breakdown. When NaCl $\geqslant$2 M, the passive film breakdown dominates the interfacial processes and the E_b decrease with increasing chloride concentration in the alkaline solution.

(2) E_b of carbon steel is linear depend on the logarithm of the chloride activity in alkaline solution. The polarizability constant (α) that correlates the potential drop across the bl/s interface is around 0.13.

(3) As predicted by the PDM, the near-normal distribution of E_b is well indicated by the near straight line in the cumulative distribution probability plot. The analysis in this study gives us a method to calculate the E_b of carbon steel in alkaline solution and its distribution for any given chloride concentration.

Table II. Parameter values used for calculating cumulative probabilities in the breakdown potential for carbon steel in deaerated alkaline solution with different chloride concentrations.

Parameters	Value	Units	Source
F, Faraday constant	96485	C mol^{-1}	Fundamental constant
R, the gas constant	8.31	J (mol K)$^{-1}$	Fundamental constant
T, the absolute temperature	298	K	Defined
N_v, Avogadro's number	6.02×10^{23}	mol^{-1}	Fundamental constant
χ, the barrier layer stoichiometry (Fe_2O_3)	3	\	Assumed
Ω, molar volume of Fe_2O_3 per cation	15.23	cm^3 mol^{-1}	From density
$\bar{D}$, the mean cation vacancy diffusivity	7×10^{-19}	cm^2 s^{-1}	From fitting
σ_D, the standard deviation for D	0.3 $\bar{D}$	cm^2 s^{-1}	From fitting
α, potential dependence of $\phi_{f/s}$	0.13		From Fig. 7
β, pH dependence of $\phi_{f/s}$	−0.01	V	Ref. 9
ε, the electric field strength	3×10^6	V cm^{-1}	Assumed
ξ, the critical vacancy concentration	5.45×10^{13}	cm^{-2}	Ref. 9
$\gamma' = \chi\alpha F/2RT$	7.60	V^{-1}	Calculated
J_m, the critical vacancy flux	3.43×10^{12}	#.cm^{-2}s^{-1}	Ref. 9
$w = \frac{\chi}{2}\Delta G_A^0 + \Delta G_S^0 - \frac{\chi}{2}F\varphi_{f/s}^0$	−14707	J mol^{-1}	Ref. 9

Acknowledgments

The authors gratefully acknowledge the support of this work by ONDRAF-NIRAS of Belgium. This work was also supported by National Key R&D Program of China (No. 2020YFC1910000).

ORCID

Jie Qiu https://orcid.org/0000-0001-7240-095X
Digby D Macdonald https://orcid.org/0000-0002-4749-9035

References

1. B. Kursten, F. Druyts, D. D. Macdonald, N. R. Smart, R. Gens, L. Wang, E. Weetjens, and J. Govaerts, *Corros. Eng. Sci. Technol.*, **46**, 91 (2011).
2. P. Lu, B. Kursten, and D. D. Macdonald, *Electrochim. Acta*, **143**, 312 (2014).
3. P. V. Marcke and W. Wacquier, *ASME 2013 15th International Conference on Environmental Remediation and Radioactive Waste Management, American Society of Mechanical Engineers* (2013).
4. J. Qiu, Y. Li, Y. Xu, A. Wu, E. Ghanbari, and D. D. Macdonald, *Corros. Sci.*, **175**, 108886 (2020).
5. V. M. Geet and E. Weetjens, *Strategic choices in the Belgian supercontainer design and its treatment in a safety case NEA-RWM-R--3-REV* (2012).
6. P. Lu, S. Sharifi-Asl, B. Kursten, and D. D. Macdonald, *J. Electrochem. Soc.*, **162**, C572 (2015).
7. P. Ghods, O. B. Isgor, F. Bensebaa, and D. Kingston, *Corros. Sci.*, **58**, 1859 (2012).
8. D. Xia, Z. Qin, S. Song, D. D. Macdonald, and J. Luo, *Corros. Commun.*, **2**, 1 (2021).
9. S. Sharifi-Asl, F. Mao, P. Lu, B. Kursten, and D. D. Macdonald, *Corros. Sci.*, **98**, 708 (2015).
10. M. Saremi and E. Mahallati, *Cem. Concr. Res.*, **32**, 1915 (2002).
11. Y. Cheng, M. Wilmott, and J. Luo, *Appl. Surf. Sci.*, **152**, 161 (1999).
12. D. D. Macdonald, J. Qiu, S. Sharifi-Asl, J. Yang, G. Engelhardt, Y. Xu, E. Ghanbari, A. Xu, A. Saatchi, and D. Kovalov, *Mater. Corros.*, **72**, 166 (2021).
13. J. Qiu, D. D. Macdonald, Y. Xu, and L. Sun, *Mater. Corros.*, **72**, 107 (2021).
14. C. Alonso, M. Castellote, and C. Andrade, *Electrochim. Acta*, **47**, 3469 (2002).
15. U. M. Angst, B. Eisner, C. K. Larsen, and O. Vennesland, *Corros. Sci.*, **53**, 1451 (2011).
16. D. D. Macdonald, J. Qiu, Y. Zhu, J. Yang, G. Engelhardt, and A. Sagüés, *Corros. Sci.*, **177**, 109018 (2020).
17. M. F. Hurley and J. R. Scully, *Corrosion*, **62**, 892 (2006).
18. R. Moster, P. Singh, L. Kahn, and K. E. Kurtis, *Corros. Sci.*, **57**, 241 (2012).
19. R. G. Duarte, A. S. Castela, R. Neves, L. Freire, and M. F. Montemor, *Electrochim. Acta*, **124**, 218 (2014).
20. G. R. Engelhardt, B. Kursten, and D. D. Macdonald, *ECS Trans.*, **58**, 35 (2014).
21. A. Alhozaimy, R. Hussain, and A. Al-Negheimish, *Cem. Concr. Compos.*, **65**, 171 (2016).
22. K. Doi, S. Hiromoto, H. Katayama, and E. Akiyama, *J. Electrochem. Soc.*, **165**, C582 (2018).
23. M. Moreno, W. Morris, M. G. Alvarez, and G. S. Duffo, *Corros. Sci.*, **46**, 2681 (2004).
24. R. Rodrigues, S. Gaboreau, J. Gance, I. Ignatiadis, and S. Betelu, *Constr. Build. Mater.*, **269**, 121240 (2020).
25. Z. Ai, J. Jiang, W. Sun, D. Song, H. Ma, J. Zhang, and D. Wang, *Appl. Surf. Sci.*, **389**, 1126 (2016).
26. B. Lin, R. Hu, C. Ye, Y. Li, and C. Lin, *Electrochim. Acta*, **55**, 6542 (2010).
27. D. D. Macdonald, *J. Electrochem. Soc.*, **139**, 3434 (1992).
28. S. Sharifi-Asl, M. Taylor, Z. Lu, G. R. Engelhardt, B. Kursten, and D. D. Macdonald, *Electrochim. Acta*, **102**, 161 (2013).
29. S. Yang and D. D. Macdonald, *Electrochim. Acta*, **52**, 1871 (2007).
30. L. F. Lin, C. Y. Chao, and D. D. Macdonald, *J. Electrochem. Soc.*, **128**, 1194 (1981).
31. Y. T. Tan, S. L. Wijesinghe, and D. J. Blackwood, *Corros. Sci.*, **88**, 152 (2014).
32. T. Shibata and T. Takeyama, *Stochastic Theory of Pitting Corrosion, Corros.*, **33**, 243 (1977).
33. D. D. Macdonald and M. Urquidi-Macdonald, *Electrochim. Acta*, **31**, 1079 (1986).